ACCEPTED VERSION

M. Sun, P. Visintin, T. Bennett

The effect of specimen size on autogenous and total shrinkage of ultra-high performance concrete (UHPC)

Construction and Building Materials, 2022; 327:126952-1-126952-10

Final publication at: http://dx.doi.org/10.1016/j.conbuildmat.2022.126952

The effect of specimen size on autogenous and total shrinkage of ultra-high performance concrete (UHPC)

M. Sun[a], P. Visintin[a*], T. Bennett[a]

[a] School of Civil, Environmental and Mining Engineering, The University of Adelaide, South Australia 5005, Australia

[*] Corresponding author.

E-mail address: phillip.visintin@adelaide.edu.au

Phone: +61 8 8313 3710

Fax: +61 8 8313 4359

Keywords: *Ultra-high performance concrete, Autogenous shrinkage, Water to binder ratio, Silica fume, Capillary tension, sample size dependency*

Abstract:

Unlike normal strength concretes, in which drying is the dominant form of shrinkage, in concretes with very low water to cement ratios autogenous and chemical shrinkage mechanisms can dominate. While the impact of specimen size and shape on drying shrinkage is well understood, the same is not true for autogenous and chemical shrinkage, and this lack of understanding may limit model precision and accuracy. To address this issue, this paper presents the results of a series of experiments conducted to measure the dependency of shrinkage of UPHC on specimen size. Results, recorded from 2 days after water addition, demonstrate a strong specimen size dependency when tested under both sealed and unsealed *conditions, thereby indicating that the underlying mechanism is fundamentally different from normal strength concrete, with autogenous shrinkage exhibiting a large influence. Existing shrinkage models (AS3600, B4, CEB-FIP, GL2000 and ACI209) are evaluated for their potential calibration and/or extension to low water to binder ratio concretes and it is shown that commonly used parameters to account for size dependency in normal strength concrete (volume to surface area ratio and hypothetical thickness) do not capture size dependency in UHPC.*

1. Introduction

Concretes with low water to binder (*w/b*) ratios, such as ultra-high performance concrete (UHPC) have been observed in some instances to exhibit larger shrinkage strains than normal strength concrete [1-6]. It has also been observed that unlike normal strength concrete in which drying is the dominant shrinkage mechanism, in UHPC, plastic and autogenous shrinkage may dominate [6-8].

The differing relative contributions of drying and autogenous shrinkage means that the applicability of existing shrinkage models, regardless of their complexity, requires investigation to ensure they are applicable or have the potential to be extended to low *w/b* ratio concretes [9]. This is necessary because existing models have, in general, been proposed and calibrated based on large datasets of normal strength concrete, and as a result they may over predict the influence of drying shrinkage [10, 11], under predict the influence of chemical and autogenous shrinkage [10, 12], underestimate the time over which shrinkage strains develop [10-12], and importantly for this work, attribute shrinkage size effect solely to the mechanism of drying [13-17] . It is therefore essential that the role of specimen size be evaluated for UHPC so that it can be adequately incorporated into future models.

Past research aimed at quantifying the mechanisms of shrinkage in normal strength concrete have identified surface free energy, capillary tension, movement of interlayer water, and disjoining pressure as the fundamental mechanisms for moisture transport and therefore drying shrinkage [9, 18, 19]. That is, drying of specimens occurs as a result of moisture transport as water diffuses out of pores and into the external environment [9]. This drying process creates an internal moisture gradient which further forces moisture transport because the coefficient of diffusion is also dependant on the moisture content [20].

The effect of specimen size on drying shrinkage of normal strength concrete has been observed across multiple studies. Hansen and Mattock [21] experimentally measured drying shrinkage of cylindrical and I-shaped cross section specimens of different sizes and found samples with larger volume to surface ratios (*v/s*) had smaller shrinkage strains and a slower rate of shrinkage. Al-Saleh and Al-Zaid [22] found that the specimen size dependency was more prominent under low environmental relative humidity, owing to the higher moisture gradients. Al-Saleh and Al-Zaid [22] and Almudaiheem and Hansen [23] also found that smaller samples had higher shrinkage rates, but sample size had no effect on the extrapolated final shrinkage magnitude.

The size effect associated with drying shrinkage can also affect the spatial variation of shrinkage within concrete specimens due to non-uniform moisture transport. For example, Campbell-Allen and Rogers [24] found that smaller specimens displayed less differential drying shrinkage and smaller final shrinkage magnitudes than in larger samples of normal strength concretes. Kim and Lee [25] reported that the internal drying shrinkage at different depths from the drying surface had significant variations and the shrinkage stresses induced by this variation may cause cracking, especially so in thick concrete structures. Zhang and Hubler [19] found the maximum thickness and the total area of cracks increase with specimen size.

With the advent of modern low water content concretes in the 1900s, autogenous shrinkage began to draw greater attention [2]. In previous research on normal and high strength concrete, the effect of specimen size on autogenous shrinkage (observed in sealed environmental conditions) is not as apparent as that associated with drying under exposure to the environment. Han and Han [26] observed a slight increase in autogenous shrinkage with specimen size in their study on high strength concrete, but dismissed this observation as potential measurement error and concluded there was no size effect on autogenous shrinkage of high strength concrete. However, Tazawa and Miyazawa [8] conversely found that that the effect of specimen size on autogenous shrinkage may not be negligible, with the underlying mechanisms being discontinuous capillary water.

Despite the very low *w/b* ratios and the dominance of autogenous shrinkage in UHPC, existing studies have not yet considered the impact that sample size may have upon on either autogenous or total shrinkage. Although across various studies shrinkage data have been obtained from samples with different sizes and shapes, it is difficult to directly compare results because of the wide variation in UHPC binders and mix designs. Also of note is the small specimen volumes considered in previous studies on UHPC, with the majority considering specimen lengths ranging from 160 mm [4, 10, 27, 28] to 1000 mm [29] and volume ranging from 25.6 cm^3 (40×40×160 mm) [4] to 9000 cm^3 (50×300×600 mm) [30]. These specimen sizes may not be large enough to evaluate UHPC shrinkage size effect, because it is possible that a smaller size effect is observed in UHPC than normal strength concrete because of the reduced importance of the drying shrinkage component. Therefore, in this study, the size effect of autogenous and total shrinkage is studied on samples with a consistent mix design and wide sample size variation.

Given the literature review has highlighted a lack of studies that take shrinkage measurements from specimens of various sizes but with a single UHPC mix design, in this paper, to better understand UHPC shrinkage size effect, autogenous and total shrinkage is measured over a 300 days period on specimens with varying *v/s* ratio, hypothetical thickness and volume. The measurements obtained are used as the basis for identifying the importance of specimen size effect in UHPC and if existing parameters used to correct for specimen size are appropriate. Finally, the potential to extrapolate existing design based shrinkage models for application to UHPC without fundamental modification is assessed. The data obtained in this study can be used as the basis for further modelling of UHPC shrinkage size effect.

2. Material and methods

In order to understand the impacts of sample size on UHPC shrinkage, different samples sizes with varying dimensions, volume to surface area (*v/s*) ratio and hypothetical thickness (t_h) were considered. Both autogenous and total shrinkage were measured to identify the shrinkage mechanism, giving rise to any size effect.

2.1 Sample size

In order to quantify sample size dependency, the sample dimensions adopted in this paper are based on *v/s*, as shown Table 1, also shown is the corresponding hypothetical thickness [16] defined as

$$t_h = \frac{2A}{P} \tag{1}$$

in which A is the cross sectional area and P is the exposed perimeter [16].

To enable easier discussion of the results, also shown in Table 1 is the sample ID, where specimens are designated first by their length, followed by their *v/s* ratio (provided to 2 significant figures), followed by the hypothetical thickness. For example, L4-22-50 represents 400 mm sample length, 22.22 mm *v/s* and 50 mm hypothetical thickness.

When considering the outcomes of testing, the first three sample dimensions with increasing *v/s* can be used to determine UHPC shrinkage sample size dependency, while the three specimens with *v/s* of 33.33 are intended to investigate the reliability of using *v/s* as a measure of shrinkage size dependency for UHPC. For each sample size, six specimens were manufactured, with three used to measure autogenous shrinkage and three to measure total shrinkage.

Table 1: Sample dimensions

Sample ID	Dimension (mm)	*v/s* (mm)	t_h (mm)	V(mm^3)
L4-22-50	100×100×400	22.22	50	4.00×10^6
L6-33-75	150×150×600	33.33	75	13.5×10^6
L8-44-100	200×200×800	44.44	100	32.0×10^6
L14-33-70	140×140×1400	33.33	70	27.44×10^6
L4-33-80	160×160×400	33.33	80	10.26×10^6

2.2 Mix design and curing

Since an investigation of the effect of material parameters on shrinkage is not the purpose of this paper, a single mix design based on the work of [12] was adopted and is shown in Table 2.

Table 2: Mix proportions by weight of UHPC

w/b	SF replacement ratio	Cement	Silica fume	Water	Sand	SP
0.17	15%	0.85	0.15	0.135	1	0.05

Two types of cementitious materials were used: a sulphate resisting cement (Type SR) and densified amorphous silica fume. According to the product data sheet [31], the components of sulphate resisting cement are 30%-50% Portland cement clinker, 50-70% ground granulated blast furnace slag (GGBFS) and 2-5% gypsum by weight, and this conforms to Australian standard AS3972-2010 [32]. Similarly, according to its product data sheet [33], the silica fume is over 89.6% silicon dioxide SiO_2, and conforms to Australian standard AS3582.3: 2016 [34]. A high range water reducing superplasticizer with retarder was used and its water content (approximately 70%) was considered to be available for hydration reaction by adding to the total water content in the mix design (i.e. the *w/b* ratio was calculated based on added water content in Table 2 and water content in superplasticizer).

The mixing of UHPC was performed in a pan mixer. The dry materials were mixed for five minutes to obtain an isotropic mix. Water was subsequently added, followed by the addition of superplasticizer, the mixing process continued for an additional 20 minutes to ensure workability. Once mixed the concrete was placed into wooden moulds, after which they were sealed by wooden covers, which were further sealed with aluminium adhesive tape to prevent moisture evaporation. The specimens in their moulds were then stored in ambient lab conditions (approximately 25℃) to cure for two days.

2.3 Shrinkage testing method

All samples were demoulded after curing, at which point half of the samples were sealed by several layers of plastic wrap for autogenous shrinkage measurement, while the remaining specimens were left with all surfaces exposed to the atmosphere. All specimens were transferred into a constant temperature and relative humidity room and measurement of original sample length were obtained.

To minimise the effect of temperature and relative humidity on shrinkage, a walk-in style constant temperature and relative humidity room set at 25℃ and 50% relative humidity was used to store all specimens during the entire measurement period. To capture any variation in environmental conditions that may occur during the period of testing a digital sensor (model SHT21) with temperature operation range of -40℃ to 125℃ and relative humidity operation range of 0%-100% was used to directly record temperature and relative humidity throughout the entire test period. The accuracies of relative humidity and temperature of the sensor are 2% and 0.3℃ respectively.

Shrinkage measurement commenced 48 hours after water addition and continued for 300 days to reach the final stage, with the intention to capture plateauing of shrinkage with time [9], during which the change in length of the specimens were recorded every 15 minutes. The shrinkage measurement zero-time was chosen based on the early-age shrinkage data in [12], where the early age shrinkage of the same mix design was measured from 3 hours after water addition. As shown in [12], UHPC shrinkage increases sharply in the first 24 hours, followed by a period of material expansion and contraction until 48 hours after water addition. This observation is a combined result of intense chemical reaction, microstructure development, ettringite formation and internal relative humidity change [12], which all can interfere the analysis of size effects.

2.4 Shrinkage testing apparatus

In order to measure UHPC shrinkage with such a wide variety of dimensions, several shrinkage measurement stands were fabricated. All six samples with the same dimensions were placed on a single stand. To enable air flow, each specimen was places on small square bars, which were themselves placed on the perforated steel bottom plate of the frame (Fig. 1). Several bolts on the bottom plate were used to adjust the entire framed to a horizontal level. On top of each sample, a spring loaded LVDT with stoke length of 10 mm and accuracy of ±0.3% was used to measure length change of the centre point of the specimen.

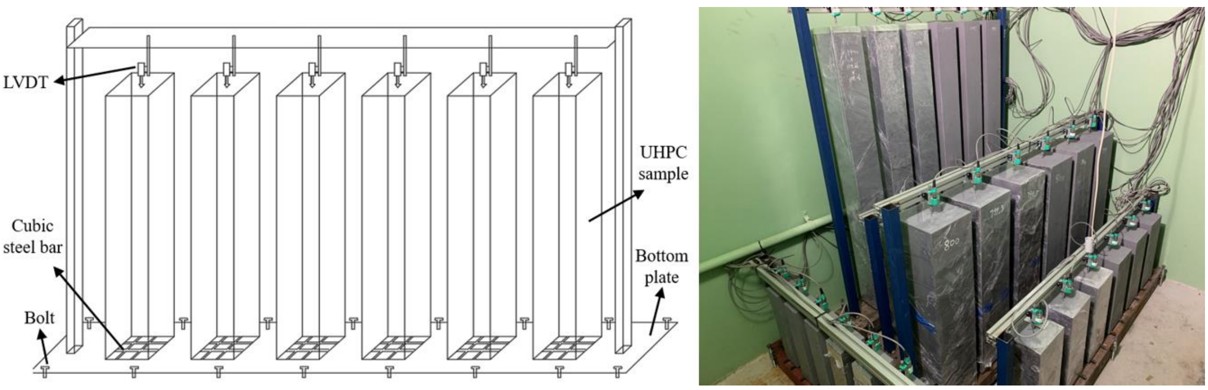

Fig. 1: Shrinkage measurement stand

3. Results and discussion

The experimentally measured test results are presented in this section, including the recorded room temperature and relative humidity and the specimen autogenous and total shrinkage.

3.1 Temperature and relative humidity

Fig. 2 shows the recorded temperature and relative humidity of the testing room, where it can be seen that the average temperature was 24.5℃ with a maximum variation of 3.5℃ .The relative humidity is approximately 50% but fluctuated by as much as ±10%.

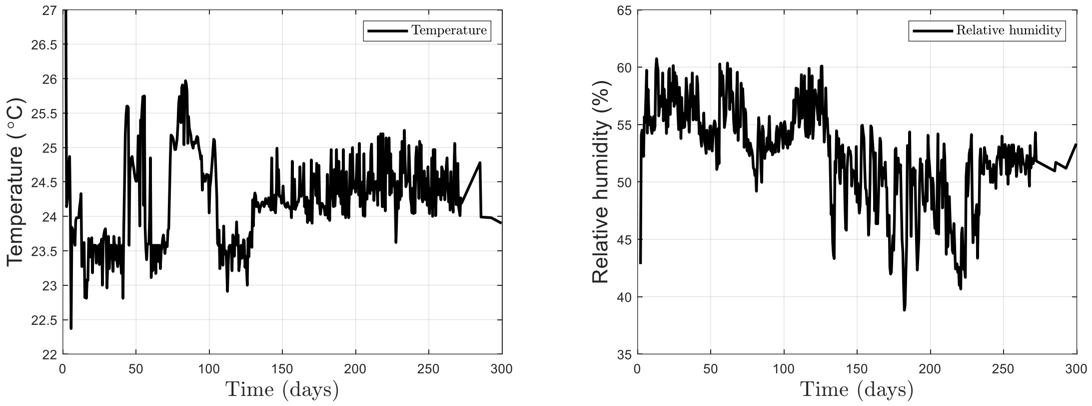

(a) (b)

Fig. 2: Testing room temperature (a) and relative humidity (b)

3.2 Shrinkage of samples with increasing *v/s*

The effect of specimen samples size on autogenous and total shrinkage is shown in in Fig. 3(a) and (b), respectively, where within each figure the solid line represents the average values of three specimens and the full scatter is shown by the grey shaded area. All results in Fig. 3 demonstrate shrinkage develops gradually with continuously decreasing rate, and the maximum scatter between the three identical specimens is approximately 50 microstrain, indicating high consistency.

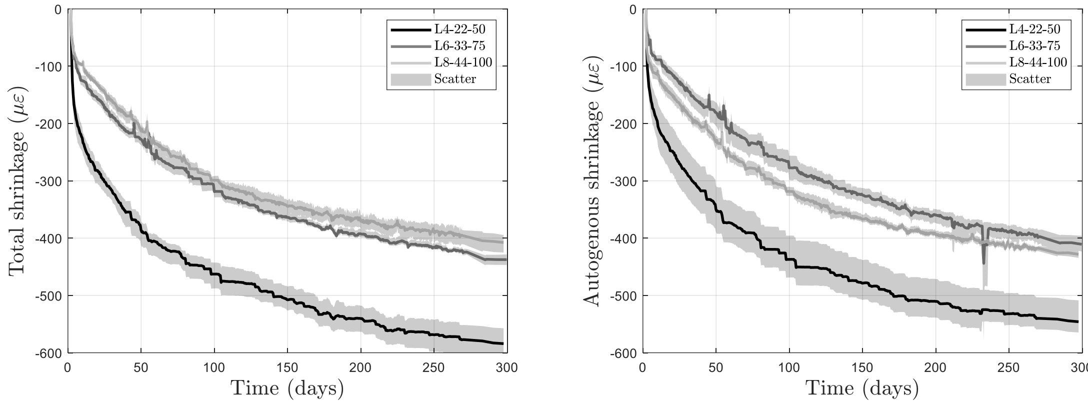

(a) (b)

Fig. 3: The effect of sample sizes (increasing *v/s*) on (a) total and (b) autogenous shrinkage strain, from 2 days after water addition

Firstly comparing Fig. 3(a) and Fig. 3(b), the variation between the magnitudes of autogenous and total shrinkage strains of each sample size is small, indicating the limited effect of drying on UHPC. Thus, it can be concluded that the shrinkage size effect observed in the UHPC total shrinkage measurements [Fig. 3(a)] is mainly due to the size effect of UHPC autogenous shrinkage, rather than non-uniform moisture gradient, caused by drying from the surface inwards.

The variation in total shrinkage strain between each specimen size is shown in Fig. 3(a), in which it can be seen that total shrinkage in UHPC has a sample size dependency, with smaller *v/s* and hypothetical thickness samples showing the higher shrinkage strain. It is however also observed in Fig. 3(a) that the total shrinkage strain does not vary in proportion with either the increment of *v/s* or hypothetical thickness of samples. For example, L4-22-50 develops much greater final total shrinkage strain at 300 days than the other samples (approximately 34% larger than L6-33-75 and 43% larger than L8-44-100), while the difference in the magnitude between L6-33-75 and L8-44-100 is relatively small, with L6-33-75 being approximately 10% larger than L8-44-100. It can however be seen in Fig. 3(a) that the total shrinkage does vary inversely proportional with specimen volume, that is the specimen with the smallest volume undergoes the largest shrinkage.

UHPC autogenous shrinkage strain in Fig. 3(b) also exhibits a sample size dependency. For example, L4-22-50 develops the largest final autogenous shrinkage strain at 300 days (approximately 27% larger than L8-44-100 and 33% larger than L6-33-75) and the other two specimen sizes (L4-22-50 and L8-44-100) display similar autogenous shrinkage strains, with L8-44-100 being approximately 4% larger than L6-33-75. This result is similar to the trend of total shrinkage strain; however, L6-33-75 shows the smallest autogenous shrinkage strain in Fig. 3(b).

Now let us consider the results in Fig. 3 in the context of existing research on normal and high strength concrete. While a finding of non-linearity in total shrinkage strain agrees with previous findings on shrinkage size dependency in normal strength and high strength concrete [21, 23, 24, 35-37], of significant difference is the mechanism of size dependency. That is, the size dependency observed in the total shrinkage measurements in Fig. 3(a) is also observed in similar magnitudes in the autogenous measurements in Fig. 3(b). This observation suggests that not only is the dominant shrinkage mechanism in UHPC autogenous shrinkage, it is also the source of the majority of the size dependent behaviour. This is in contrast to normal and high strength concrete, in which the final autogenous shrinkage strain is generally at least one order of magnitude smaller than total shrinkage strain and size dependency is observed under drying conditions because of non-uniform moisture transport [12] under drying conditions. Furthermore, although the non-linear behaviour with the increase in *v/s* was observed by Campbell-Allen and Rogers [24] and Almudaiheem and Hansen [23] on small prismatic samples of normal strength concrete, the magnitude in non-linearity in this paper is much larger than previously observed. This may be due to the much larger sample size adopted in this series of tests, leading to slower shrinkage rates [36, 38]; this however cannot be confirmed, because the 300 days test period is not long enough for UHPC samples of this size to reach their ultimate shrinkage strains.

3.3 Shrinkage of samples with constant *v/s*

The total and autogenous shrinkage strains of samples with identical *v/s* ratio can be seen in Fig. 4(a) and (b), respectively. The solid lines are averaged shrinkage strains of three samples, with the grey shaded area being scatter. Again, it can be seen that the scatter of each sample size is relatively small, compared to the magnitude of final shrinkage value at 300 days, with the maximum scatter being less than 50 microstrain.

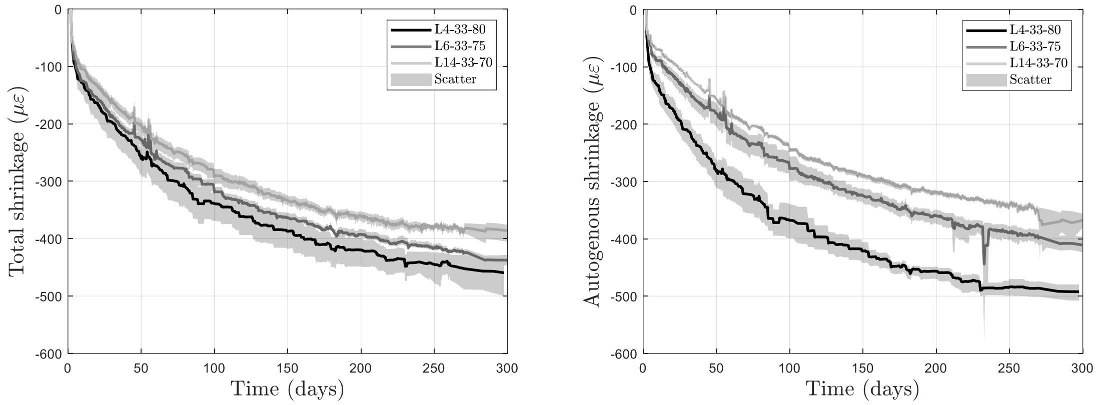

(a) (b)

Fig. 4: The effect of different sample dimensions with constant *v/s* on: (a) total and (b) autogenous shrinkage, from 2 days after water addition

In Fig. 4: The effect of different sample dimensions with constant *v/s* on: (a) total and (b) autogenous shrinkage, from 2 days after water addition

(a), specimen L4-33-80 demonstrates the largest final total shrinkage strain at 300 days and this is approximately 5% larger than that observed for L6-33-75 and 20% larger than that observed for L14-33-70. Given that all specimens in Fig. 3(a) have the same *v/s* ratio but up to a 20% difference in the final recorded shrinkage strain it is suggested here that the *v/s* ratio does not fully capture the size dependency of total shrinkage strain in UHPC. Also observed in Fig. 4(a) is that the larger total shrinkage strains are developed in samples with larger hypothetical thickness, and this is opposite to what is observed in Fig. 3(a) where the largest shrinkage strains were observed in samples with the smallest hypothetical thickness. This variation in behaviour may be because sample length is omitted in the calculation of hypothetical thickness with only cross-section area being considered. That is, although the samples in Fig. 4(a) have the same *v/s*, because of their varied length, the overall volume is different. Interestingly, the results observed here suggest that neither the *v/s* nor the hypothetical thickness captures size effect in UHPC shrinkage and that the element volume alone may be a better measure. This outcome can likely be explained by the dominance of autogenous shrinkage over drying shrinkage in UHPC, which diminishes the impact of the exposed surface area and promotes the impact of specimen volume in the mechanisms that drive autogenous shrinkage (available water and heat generated).

The autogenous shrinkage strains in Fig. 4(b) show the same trend as total shrinkage, however, the difference in magnitude between L4-33-80 and the other two sizes is much larger than that of total shrinkage. For example, the largest autogenous shrinkage strain at 300 days, for specimen L4-33-80 is approximately 20% larger than that observed in L6-33-75 and 38% larger than that observed in L14-33-70. Similar to what was observed for total shrinkage, these results generally align with the volume of the samples (L4-33-80 being the smallest and L14-33-70 being the largest) and suggest that specimen volume may be a more appropriate measure of size dependency for shrinkage of UHPC.

3.4 Shrinkage of all sample sizes

To help further identify an appropriate indicator of specimen size dependency all experimental observations are plotted on a single graph with log scale in Fig. 5. As discussed for Fig. 3 and

Fig. 4, there is no clear trend in either total or autogenous shrinkage with either *v/s* or hypothetical thickness, but there does appear to be a general trend with overall specimen volume. That is, when considering total shrinkage in Fig. 5(a) the results, ranked from highest shrinkage strains to lowest shrinkage strains, at 300 days correspond to the ranking of specimen volume (Table 1) from smallest to largest. The same general trend is seen in the results for autogenous shrinkage in Fig. 5(b) with the exception of the L8-44-100 specimen, which is out of sequence when ranked according to volume.

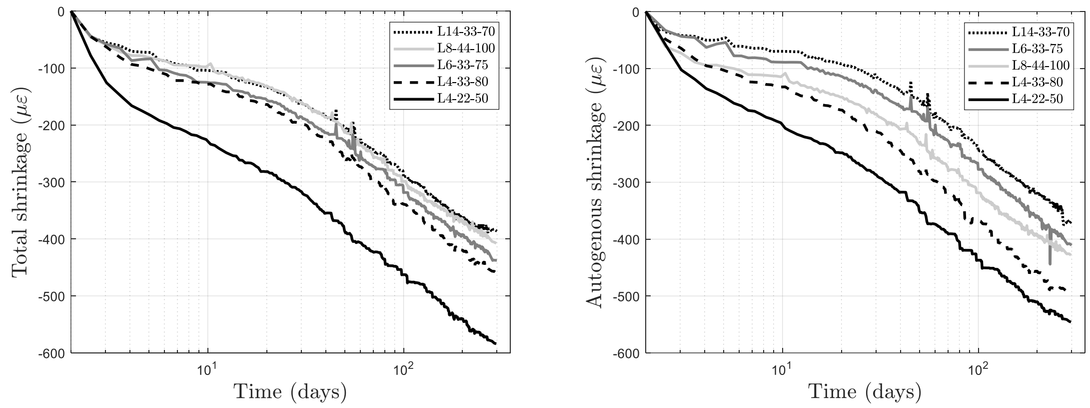

(a) (b)

Fig. 5: (a) Total and (b) autogenous shrinkage strains of all sample sizes, measured from 2 days after water addition

When interpreting the results in Fig. 5 the size dependency of UHPC autogenous shrinkage is greater than that of total shrinkage. It can also be seen that the measured autogenous shrinkage is larger than measured total shrinkage for some sample sizes. For example, L4-33-80 has approximately 50 microstrain larger autogenous shrinkage than total shrinkage at 300 days. As each line is average of 3 individually measured samples, this observation can be partially attributed to experimental scatter. Variation can also be expected because moisture loss due to evaporation under drying conditions has a greater potential to occur at early ages [12] when the variation in internal and external humidity is the greatest and this can trigger competing effects. For example, moisture evaporation can reduce water available for hydration leading to decrease in both chemical and autogenous shrinkage, especially for UHPC with low water contents. At the same time, increased water loss results in higher drying shrinkage. Further, the exothermal heat generated during hydration and the constant temperature boundary conditions give rise to non-uniform internal temperature distributions [12] which feedback to influence rate of reaction, heat transfer and moisture transport processes.

In addition the these mechanism, a non-uniform distribution of the degree of reaction can form due to the variation of temperature at different locations, leading to two competing effects. Water consumed in the hydration and pozzolanic reactions of the binders reduces the internal relative humidity, resulting in increased capillary stress and autogenous shrinkage. At the same time the accelerated chemical reaction, resulting from heat accumulation can promote the development UHPC matrix stiffness, reducing autogenous shrinkage. Based on the test results, as shown in Fig. 5(b), samples with smaller volume and length show larger autogenous shrinkage strains, indicating that the retarding effect of matrix stiffness development is greater that the expedition effect of accelerated chemical reaction. Therefore, the time dependent heat transfer and moisture transport processes are able to induce a specimen size dependency even without moisture exchange with an external environment.

4. Shrinkage size effect modelling

Several highly calibrated design models are available to predict shrinkage in normal and high strength concrete (e.g. CEB-FIP [13], GL2000 [14] and ACI209 [15], AS3600 [16] and B4 [17]). With the exception of AS3600 [16] and B4 [17] these approaches typically only consider total shrinkage and do not separate the differing components of shrinkage. Although suggested by the form of AS3600 and B4, drying and autogenous shrinkage components are not directly additive [9]. For normal and high strength concrete, this does not present a significant challenge because the ultimate drying shrinkage is generally an order of magnitude larger than the ultimate autogenous shrinkage, but this is not the case for UHPC and therefore further review of the coupling of autogenous and drying shrinkage may be required. Also of significance in AS3600 [16] and B4 [17] is that modifiers for specimen shape and size are only present on the drying shrinkage components such that it is assumed that significant size dependency only arises from moisture diffusion during drying rather than from any mechanism that occurs under sealed conditions. As shown in the results of this study, and also in [10-12], this assumption is problematic because drying is in general highly limited in UHPC because of the low *w/b* ratio and dense microstructure [10], and the drying shrinkage that does occur is generally limited to the first few days after water addition [8].

Despite these challenges with existing models, in order to assess their performance when extrapolated for application to UHPC Fig. 6(a) presents a comparison of AS3600 [16] and B4 [17] predicted and observed autogenous shrinkage, and Figs. 6(b)-(f) present a comparison of GL2000 [14] and ACI209 [15], AS3600 [16] and B4 [17] predicted and observed total shrinkage. The main equations and parameters of each model are described below using their own nomenclature. The values of each parameter can be seen in Table 3.

AS3600

The Australian standard for concrete design AS3600 [16] decomposes the total strain ε_{cs} as the sum of autogenous and drying components

$$\varepsilon_{cs} = \varepsilon_{cse} + \varepsilon_{csd} \tag{2}$$

where ε_{cs} is predicted shrinkage strain, ε_{cse} is autogenous shrinkage strain and ε_{csd} is drying shrinkage strain. The autogenous shrinkage strain can be calculated as

$$\varepsilon_{cse} = \varepsilon_{cse}^{*} \times (1 - e^{-0.07t}) \tag{3}$$

where $\varepsilon_{cse}^{*} = \varepsilon_{cse}^{*}(f_c)$ is ultimate autogenous shrinkage strain, which is a function of compressive strength f_c and t is time after setting.

The drying shrinkage strain is calculated as

$$\varepsilon_{csd} = k_1 k_4 \varepsilon_{csd.b} \tag{4}$$

where $k_1 = k_1(t_h, t_d)$ is a function of drying time t_d and hypothetical thickness t_h, k_4 is environment factor and $\varepsilon_{csd.b} = \varepsilon_{csd.b}(f_c)$ is basic drying shrinkage strain, which is formulated as a function of compressive strength f_c.

B4

The B4 model [17] for creep and shrinkage of concrete, also treats the autogenous and drying shrinkage strains as being additive to produce a total strain $\epsilon_{sh,total}(t, t_0)$

$$\epsilon_{sh,total}(t, t_0) = \epsilon_{au}(t, t_0) + \epsilon_{sh}(t, t_0) \tag{5}$$

$\epsilon_{au}(t, t_0)$ and $\epsilon_{sh}(t, t_0)$ are the autogenous and drying shrinkage strains, respectively, t is the age of concrete and t_0 is age at which drying begins. The autogenous shrinkage strain can be calculated as

$$\epsilon_{au}(t, t_0) = \epsilon_{au\infty} \left[1 + \left(\frac{\tau_{au}}{t + t_0}\right)^{\alpha}\right]^{r_t} \tag{6}$$

where $\epsilon_{au\infty} = \epsilon_{au\infty}\big(a/c, w/c, \epsilon_{au,cem}, r_{\epsilon a}, r_{\epsilon w}\big)$ is ultimate autogenous shrinkage strain, that is a function of the aggregate to cement ratio a/c, water to cement ratio w/c and cement type related parameters $\epsilon_{au,cem}$, $r_{\epsilon a}$ and $r_{\epsilon w}$. $\tau_{au} = \tau_{au}\big(w/c, \tau_{au,cem}, r_{\tau w}\big)$ is the autogenous shrinkage halftime, which is in turn defined as a function of water to cement ratio w/c and cement type related parameters $\tau_{au,cem}$ and $r_{\tau w}$. $\alpha = \alpha(w/c, r_{\alpha})$ is a function of the water to cement ratio w/c and cement type related parameter r_α. The power term r_t is also a parameter related to the cement type.

The drying shrinkage strain is calculated as

$$\epsilon_{sh}(t,t_0) = \epsilon_{sh\infty}(t_0) k_h \mathrm{S}(t) \tag{7}$$

where $\epsilon_{sh\infty}(t_0)$ is a function of t_0, aggregate to cement ratio a/c, water to cement ratio w/c, cement content, mass density, compressive strength, aggregate dependent parameter $k_{\epsilon a}$ and cement type related parameters ϵ_{cem}, $p_{\epsilon a}$, $p_{\epsilon w}$, $p_{\epsilon c}$. $k_h = k_h(h)$ is a function of relative humidity h and $\mathrm{S}(t)$ is a function of t, t_0, aggregate to cement ratio a/c, water to cement ratio w/c, cement content, mass density, cement type related parameters τ_{cem}, $p_{\tau a}$, $p_{\tau w}$, $p_{\tau c}$, aggregate dependent parameter $k_{\epsilon a}$ and shape parameter k_s.

ACI209

The ACI model of concrete shrinkage predicts the total shrinkage $\varepsilon_{sh}(t,t_c)$

$$\varepsilon_{sh}(t,t_c) = \frac{t - t_c}{T_c + (t - t_c)} \varepsilon_{shu} \tag{8}$$

where t is the age of concrete, t_c is the age when drying begins, T_c is curing method parameter, being 35 for moist curing and 55 for steam curing and ε_{shu} is ultimate shrinkage strain, being 780×10^{-6} with a correction factor γ_{sh} for conditions other than standard conditions which can be calculated by

$$\gamma_{sh} = \gamma_{sh,tc}\gamma_{sh,RH}\gamma_{sh,vs}\gamma_{sh,s}\gamma_{sh,\psi}\gamma_{sh,c}\gamma_{sh,\alpha} \tag{9}$$

where $\gamma_{sh,tc}$ is correction factor for initial moist curing, $\gamma_{sh,RH}$ is correction factor for ambient relative humidity, $\gamma_{sh,vs}$ is correction factor for size, $\gamma_{sh,s}$ is correction factor for slump, $\gamma_{sh,\psi}$ is correction factor for fine aggregate, $\gamma_{sh,c}$ is correction factor for cement content and $\gamma_{sh,\alpha}$ is correction factor for air content.

CEB-FIP

Total shrinkage at time t when drying begins at time t_c is

$$\varepsilon_{sh}(t, t_c) = \varepsilon_{sho}\beta_s(t - t_c) \tag{10}$$

where, $\varepsilon_{sho} = \varepsilon_{sho}(\beta_{sc}, f_c, h)$ is notional shrinkage coefficient, calculated by cement type parameter β_{sc}, strength f_c and relative humidity h, β_s is a function of effective thickness t_h.

GL2000

$$\varepsilon_{sh}(t, t_c) = \varepsilon_{shu}(1 - 1.18h^4)\sqrt{\frac{t - t_c}{t - t_c + 0.15(v/s)^2}} \tag{11}$$

where $\varepsilon_{sh}(t, t_c)$ is predicted total shrinkage, t is age of concrete, t_c is age when drying begins, v/s is volume to surface ratio, h is relative humidity, $\varepsilon_{shu} = \varepsilon_{shu}(f_c, K)$ is ultimate shrinkage, calculated by strength f_c and cement type parameter K.

Table 3: Parameter values of each model

Model	Parameter	Description	Value	Source
AS3600	ε^*_{cse}	Ultimate autogenous shrinkage strain, calculated by compressive strength	4.9×10^{-4}	[16], Eq. 3.1.7.2 (3)
	$\varepsilon_{csd.b}$	Basic drying shrinkage strain, calculated by compressive strength and $\varepsilon^*_{csd.b}$=800e-6, given by [16]	1.8×10^{-4}	[16], Eq. 3.1.7.2 (5)
	k_1	Size related parameter, calculated by sample size and time	Value changes with time.	[16], Fig. 3.1.7.2
	k_4	Environment parameter, chosen according to the environment	0.65 for interior environment	[16], Eq. 3.1.7.2 (4)
B4	τ_{cem}	Cement type dependent parameter for drying shrinkage, chosen based on hardening speed (normal hardening speed concrete adopted)	0.016	[17], Table 1
	$p_{\tau a}$		-0.33	
	$p_{\tau w}$		-0.06	
	$p_{\tau c}$		-0.1	
	ϵ_{cem}		360×10^{-6}	
	$p_{\epsilon a}$		-0.8	
	$p_{\epsilon w}$		1.1	
	$p_{\epsilon c}$		0.11	
	$\tau_{au,cem}$	Cement type dependent parameter for autogenous shrinkage, chosen based on hardening speed (normal hardening speed concrete adopted)	1	[17], Table 2
	$r_{\tau w}$		3	
	r_t		-4.5	
	r_a		1	
	$\epsilon_{au,cem}$		210×10^{-6}	
	$r_{\epsilon a}$		-0.75	
	$r_{\epsilon w}$		-3.5	
	k_s	Shape parameter, chosen based on sample shape	1.25 for infinite square prism	[17], Eq. (23)
	$k_{\epsilon a}$	Aggregate dependent parameter, chosen based on aggregate type	1 for no information on aggregate type exists	[17], Table 6

	$\times\,\tau_{cem}$	Admixture dependent parameter scaling factors for τ_{cem}, $\epsilon_{au,cem}$, $r_{\epsilon w}$ and r_a, chosen based on admixture type and dosage (Silica fume>8%, ≤18% mass of cement adopted)	2.6	[17], Table 4
	$\times\,\epsilon_{au,cem}$		0.82	
	$\times\,r_{\epsilon w}$		0	
	$\times\,r_a$		1.2	
ACI209	T_c	Curing method parameter	35 for moist curing	[15]
	ε_{shu}	Ultimate shrinkage strain, being 780e-6 under standard conditions, considering correction factor for conditions other than standard conditions	$780\times 10^{-6}\times\gamma_{sh}$	[39] Eq. (A-4)
	γ_{sh}	Correction factor ultimate shrinkage strain	0.87 for *v/s*=22.22 0.82 for *v/s*=33.33 0.78 for *v/s*=44.44	[39] Eq. (A-5) to (A-14)
CEB-FIP	ε_{sho}	Notional shrinkage coefficient	9.49×10^{-5}	[40], Eq. (3)
	β_{sc}	Cement type parameter. Given type SR cement has no information, type I cement was adopted.	5 for type I cement	[40]
	β_s	Size and time dependent parameter	Value changes with time.	[40], Eq. (5)
GL2000	ε_{shu}	Ultimate shrinkage, calculated by cement type parameter, compressive strength and relative humidity	4.70×10^{-4}	[40], Eq. (14)
	K	Cement type parameter. Given type SR cement has no information, type I cement was adopted.	1 for type I cement	[40]

The results of this comparison in Fig. 6(a) show that neither AS3600 [16] and B4 [17] can adequately capture autogenous shrinkage in UHPC without recalibration. The B4 model captures the shape, but overestimates the experimental results for all sample sizes with no sample size correction included for autogenous shrinkage. Autogenous shrinkage plateaus before 100 days using the Australian Standard AS3600 also has no sample size correction, this plateau is however the result of the underestimate of the ultimate autogenous shrinkage strain rather than the functional form of the equation.

The comparison of model result for total shrinkage by AS3600, B4, GL2000 and ACI209, for all sample sizes is shown in Fig. 6(b)-(f). As would be expected the fit is generally poor, with the exception of GL2000, which is an empirical approach and appears to be better suited to extrapolate based on compressive strength in its current form. It should also be noted that no comparison to CEB-FIP could be undertaken because the approach is calibrated between 12 to 80 MPa and extrapolation beyond this range yielded nonsensical outputs. Regarding the potential to extrapolate existing models, it can be seen in Fig. 6 that although each model has minor differences in form, all generally produce the same overall shape and so all have the potential to be recalibrated from the perspective of creating a simple expression for application in design. However for the development of an approach that captures the underlying physics, the coupling of all shrinkage mechanisms will need to be reconsidered for UHPC given the increased significance of those driven by chemical reactions.

It should be noted that retarder, included in the superplasticizer, can also affect shrinkage and only B4 model considers retarder as parameter scaling factor, as given in Table 4 of [17]. However, when considering the combined effect of silica fume, retarder and superplasticizer, the lack of scaling factor requires further study and calibration.

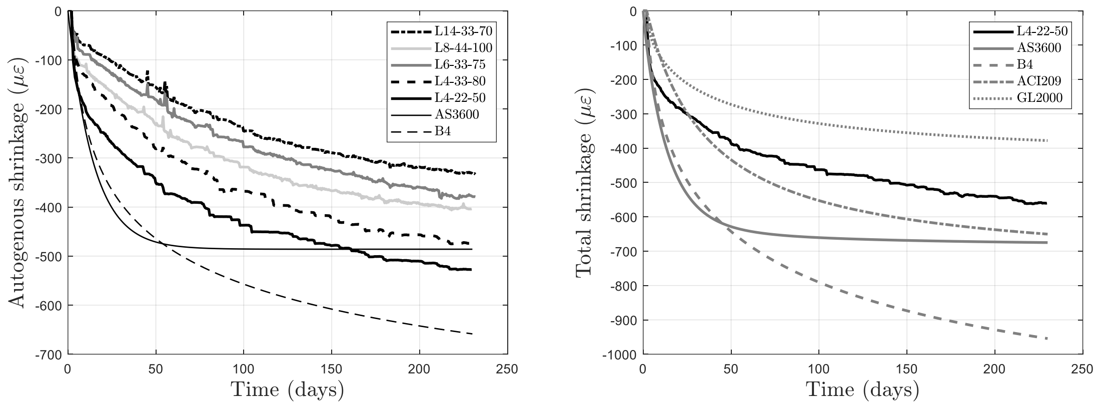

(a) (b)

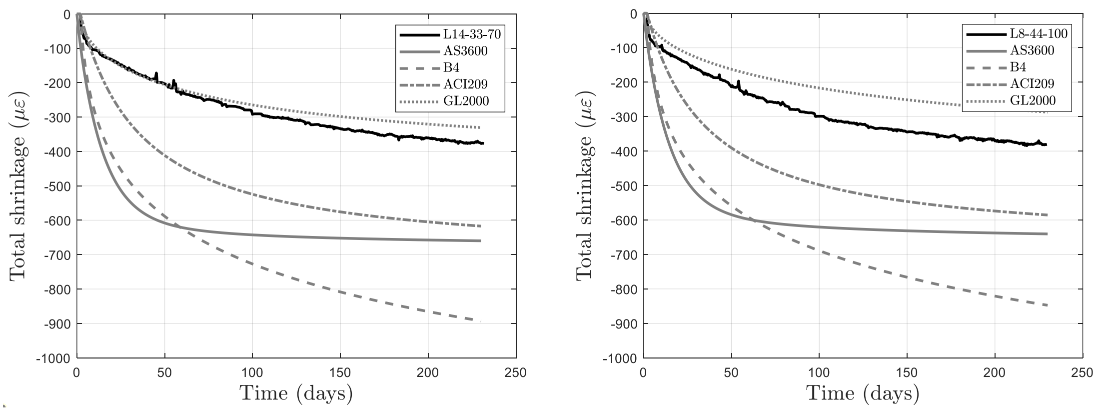

(c) (d)

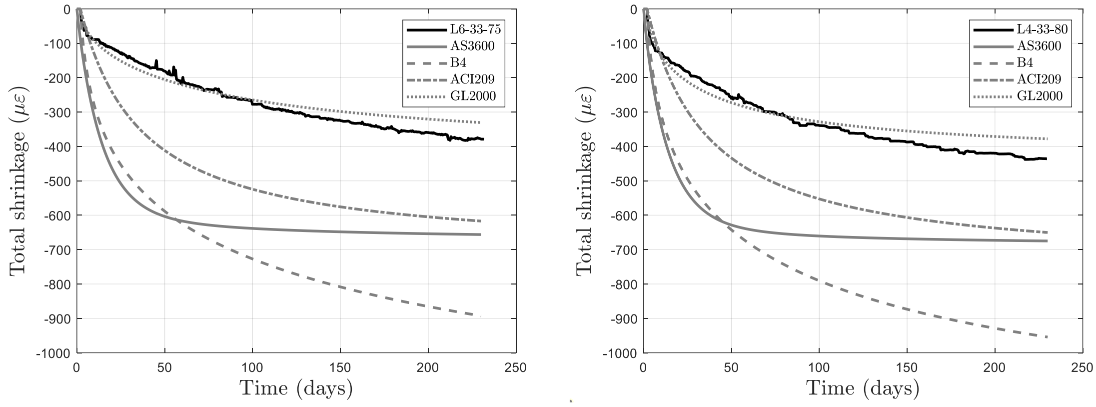

(e) (f)

Fig. 6: Comparison between test results and design codes, (a): autogenous shrinkage (b)-(f): total shrinkage

In future modelling work it is necessary to consider how to introduce a size effect to autogenous shrinkage, this is not a simple problem and will likely require the consideration of binder reactivity and the corresponding chemical shrinkage, temperature distribution due to hydration and pozzolanic reaction and heat exchange, moisture transfer and capillary tension and the interactions between them.

Further challenges in model development exist because of the limited length of existing test observations, that is despite 300 days of experimental observation, when plotted on a log-scale, it can be observed in Fig. 5 that shrinkage strains have not yet plateaued meaning that models requiring a shrinkage half-time or ultimate shrinkage magnitude may result in an ill-conditioned problem [9]. Short testing periods appear to be extremely common when considering UHPC with the vast majority of testing being conducted over a 7-day observation period (e.g. [5, 44-48]) thereby limiting the ability to broadly calibrate models.

In order to develop a unified model that can be used overall strength grades, further work is also required to identify the tipping point at which autogenous shrinkage begins to dominate drying shrinkage and where a strong autogenous shrinkage size effect begins to appear.

5. Conclusions

Unlike normal strength concretes in which drying is the dominant form of shrinkage, in concretes with a very low water to cement ratios autogenous and chemical shrinkage mechanisms can dominate. Although the impact of specimen size and shape on drying shrinkage is well understood for normal strength concrete, the same is not true for autogenous and chemical shrinkage, and this lack of understanding may limit model precision and accuracy, particularly for UHPC. To address this issue, an experimental study was conducted to measure shrinkage strains on UHPC elements with large variations in size and with large variations in size but identical *v/s* ratios and the following conclusions can be drawn from this research:

- Size dependency of shrinkage strains in UHPC has not previously been measured and both the highly variable binder type and limited variation in specimen size investigated in previous studies makes drawing conclusions from the compilation of previous studies difficult.
- The difference between total and autogenous shrinkage in UHPC is small, indicating negligible drying shrinkage occurred in UHPC mixes due to limited water content and dense microstructure. This implies the modelling of UHPC shrinkage and its size dependency cannot be captured using the same approaches employed for normal and high strength concretes.
- The description of sample dependent shrinkage in UHPC is not adequately described by volume to surface area (*v/s*) scaling - significant variations in shrinkage strains are observed when *v/s* is constant.
- Given that autogenous shrinkage is the dominant shrinkage mechanism, which is not driven by interactions with the surrounding environment, the use of volume alone may be a better mechanism to scale for specimen size. Further research is required in this area to investigate samples that have larger variations in volume, that is, although the

specimens tested in this campaign had widely varying cross sections and lengths, their overall volume was all in the same order of magnitude except for specimen L4-22-50 which was observed to have significantly larger shrinkage strains than the remaining specimens.

- The existing shrinkage models, such as B4, AS3600, ACI209, CEB-FIP and GL2000, are not presently capable of modelling UHPC shrinkage size effect, as these models attribute shrinkage size effect to drying shrinkage, which is opposite to UHPC. Given that, B4, AS3600 and GL2000 utilise *v/s* to scale and describe shrinkage size effect for normal and high strength concrete, it can be expected that these models will require fundamental modifications if they are to be extended to UHPC.

Acknowledgements

This material is based upon work supported by the Australian Research Council Discovery Project 190102650

References

[1] H. Huang, G. Ye, Examining the “time-zero” of autogenous shrinkage in high/ultra-high performance cement pastes, Cement and Concrete Research 97 (2017) 107-114.

[2] O.M. Jensen, P.F. Hansen, Autogenous deformation and RH-change in perspective, Cement and Concrete Research 31(12) (2001) 1859-1865.

[3] D. Shen, J. Jiang, J. Shen, P. Yao, G. Jiang, Influence of curing temperature on autogenous shrinkage and cracking resistance of high-performance concrete at an early age, Construction and Building Materials 103 (2016) 67-76.

[4] P. Shen, L. Lu, Y. He, M. Rao, Z. Fu, F. Wang, S. Hu, Experimental investigation on the autogenous shrinkage of steam cured ultra-high performance concrete, Construction and building materials 162 (2018) 512-522.

[5] A. Soliman, M. Nehdi, Effect of partially hydrated cementitious materials and superabsorbent polymer on early-age shrinkage of UHPC, Construction and Building Materials 41 (2013) 270-275.

[6] T. Xie, C. Fang, M.M. Ali, P. Visintin, Characterizations of autogenous and drying shrinkage of ultra-high performance concrete (UHPC): An experimental study, Cement and Concrete Composites 91 (2018) 156-173.

[7] J. Liu, N. Farzadnia, C. Shi, X. Ma, Effects of superabsorbent polymer on shrinkage properties of ultra-high strength concrete under drying condition, Construction and Building Materials 215 (2019) 799-811.

[8] E.-i. Tazawa, S. Miyazawa, Experimental study on mechanism of autogenous shrinkage of concrete, Cement and Concrete Research 25(8) (1995) 1633-1638.

[9] Z.P. Bažant, M. Jirásek, Creep and hygrothermal effects in concrete structures, Springer2018.

[10] S.-H. Kang, S.-G. Hong, J. Moon, Shrinkage characteristics of heat-treated ultra-high performance concrete and its mitigation using superabsorbent polymer based internal curing method, Cement and Concrete Composites 89 (2018) 130-138.

[11] C. Fang, M. Ali, T. Xie, P. Visintin, A.H. Sheikh, The influence of steel fibre properties on the shrinkage of ultra-high performance fibre reinforced concrete, Construction and Building Materials 242 (2020) 117993.

[12] M. Sun, T. Bennett, P. Visintin, Plastic and early-age shrinkage of Ultra-high performance concrete (UHPC): experimental study of the effect of water to binder ratios, silica fume dosages under controlled curing conditions, Online ahead of print (2021) https://doi.org/10.1016/j.cscm.2022.e00948.

[13] C.E.-I.d. Béton, CEB-FIP model code 1990: Design code, Thomas Telford Publishing1993.

[14] N. Gardner, M. Lockman, Design provisions for drying shrinkage and creep of normal-strength concrete, Materials journal 98(2) (2001) 159-167.

[15] H. Nassif, N. Suksawang, M. Mohammed, Effect of curing methods on early-age and drying shrinkage of high-performance concrete, Transportation research record 1834(1) (2003) 48-58.

[16] AS 3600:2018 Concrete structures, Standards Australia, 2018.

[17] Z.P. Bazant, M. Jirasek, M. Hubler, I. Carol, RILEM draft recommendation: TC-242-MDC multi-decade creep and shrinkage of concrete: material model and structural analysis. Model B4 for creep, drying shrinkage and autogenous shrinkage of normal and high-strength concretes with multi-decade applicability, Materials and structures 48(4) (2015) 753-770.

[18] W. Hansen, Drying shrinkage mechanisms in Portland cement paste, Journal of the American Ceramic society 70(5) (1987) 323-328.

[19] Y. Zhang, M. Hubler, Role of early drying cracks in the shrinkage size effect of cement paste, Journal of Engineering Mechanics 146(11) (2020) 04020128.

[20] K. Sakata, A study on moisture diffusion in drying and drying shrinkage of concrete, Cement and Concrete Research 13(2) (1983) 216-224.

[21] T.C. Hansen, A.H. Mattock, Influence of Size and Shape of Member on the Shrinkage and Creep of Concrete, Journal Proceedings, 1966, pp. 267-290.

[22] S.A. Al-Saleh, R.Z. Al-Zaid, Effects of drying conditions, admixtures and specimen size on shrinkage strains, Cement and concrete research 36(10) (2006) 1985-1991.

[23] J.A. Almudaiheem, W. Hansen, Effect of specimen size and shape on drying shrinkage of concrete, Materials Journal 84(2) (1987) 130-135.

[24] D. Campbell-Allen, D.F. Rogers, Shrinkage of concrete as affected by size, Matériaux et Construction 8(3) (1975) 193-202.

[25] J.-K. Kim, C.-S. Lee, Prediction of differential drying shrinkage in concrete, Cement and Concrete Research 28(7) (1998) 985-994.

[26] B. Persson, D.P. Bentz, G. Fagerlund, Self-desiccation and its importance in concrete technology: Proceedings of the fourth international research seminar, Gaithersburg, Maryland, USA, June 2005, Division of Building Materials, LTH, Lund University2005.

[27] P. Li, H. Brouwers, W. Chen, Q. Yu, Optimization and characterization of high-volume limestone powder in sustainable ultra-high performance concrete, Construction and Building Materials 242 (2020) 118112.

[28] S. Li, S. Cheng, L. Mo, M. Deng, Effects of steel slag powder and expansive agent on the properties of ultra-high performance concrete (UHPC): based on a case study, Materials 13(3) (2020) 683.

[29] X. Zhang, Z. Liu, F. Wang, Autogenous shrinkage behavior of ultra-high performance concrete, Construction and Building Materials 226 (2019) 459-468.

[30] Y. Zhu, Y. Zhang, H.H. Hussein, J. Liu, G. Chen, Experimental study and theoretical prediction on shrinkage-induced restrained stresses in UHPC-RC composites under normal curing and steam curing, Cement and Concrete Composites 110 (2020) 103602.

[31] Product Data Sheet SULFATE RESISTING CEMENT, Adelaide Brighton Cement Ltd (2018).

[32] AS 3972-2010 General purpose and blended cements, Standards Australia, 2010.

[33] ECOTEC SILICA FUME DATASHEET, ECOTEC silica fume (2012).

[34] AS/NZS 3582.3:2016 Supplementary cementitious materials, Part 3: Amorphous silica, Standards Australia / Standards New Zealand, 2016.

[35] Y. Ohama, S. Kan, Effects of specimen size on strength and drying shrinkage of polymer-modified concrete, International Journal of Cement Composites and Lightweight Concrete 4(4) (1982) 229-233.

[36] K. Van Breugel, H. Ouwerkerk, J. De Vries, Effect of mixture composition and size effect on shrinkage of high strength concrete, Proc. Int. RILEM Workshop Shrinkage of Concrete-Shrinkage, 2000, pp. 161-177.

[37] A.H. Bryant, C. Vadhanavikkit, Creep, shrinkage-size, and age at loading effects, Materials Journal 84(2) (1987) 117-123.

[38] P. Lura, K.v. Breugel, AUTOGENOUS AND DRYING SHRINKAGE OF HIGH STRENGTH LIGHTWEIGHT AGGREGATE CONCRETE AT EARLY AGES THE EFFECT OF SPECIMEN SIZE, 2010.

[39] C. Videla, D.J. Carreira, N. Garner, Guide for modeling and calculating shrinkage and creep in hardened concrete, ACI report 209 (2008).

[40] S.A. Al-Saleh, Comparison of theoretical and experimental shrinkage in concrete, Construction and Building Materials 72 (2014) 326-332.